PLASMONICS

Electrically switchable metallic polymer nanoantennas

Julian Karst[1], Moritz Floess[1], Monika Ubl[1], Carsten Dingler[2], Claudia Malacrida[2], Tobias Steinle[1], Sabine Ludwigs[2], Mario Hentschel[1], Harald Giessen[1]*

Electrical switching of a metal-to-insulator transition would provide a building block for integrated electro-optically active plasmonics. In this work, we realize plasmonic nanoantennas from metallic polymers, which show well-pronounced localized plasmon resonances in their metallic state. As a result of the electrochemically driven optical metal-to-insulator transition of the polymer, the plasmonic resonances can be electrically switched fully off and back on at video-rate frequencies of up to 30 hertz by applying alternating voltages of only ±1 volt. With the use of this concept, we demonstrate electrically switchable beam-steering metasurfaces with a 100% contrast ratio in transmission. Our approach will help to realize ultrahigh efficiency plasmonic-based integrated active optical devices, including high-resolution augmented and virtual reality technologies.

Miniaturization of optical components is key for achieving ultimate spatiotemporal control of light, which will in turn enable researchers to facilitate and improve emerging optical technologies such as augmented and virtual reality, dynamic holography, LIDAR (light detection and ranging), and high-resolution wavefront and polarization shapers. Subwavelength nanoantennas are a prime candidate to achieve this goal (*1*–*5*). Their resonant nature allows highly efficient interaction with light and can locally enhance the manipulation, detection, or modulation of light on ultrasmall, subwavelength scales. The advent of metasurfaces has provided tools with which to realize plasmon-based spatially dependent static light control on nanometer scales (*6*–*8*). These include ultrathin optical elements, such as metalenses (*9*, *10*), made from metals as well as dielectrics for generalized amplitude and phase control (*11*, *12*). Integration into dynamic electro-optical components requires active spatiotemporal light control with nanoantennas via a dynamic change of the optical properties upon an external stimulus (*13*, *14*). One possibility is to operate nanoantennas close to a phase transition, thus resulting in switchable plasmonic resonances and active metasurfaces with high contrast ratios (*15*, *16*). Such direct modifications rely on structural or chemical material transitions stimulated by chemical reactions (*15*), gas exposure (*17*, *18*), or temperature (*19*, *20*). They are usually slow, with incomplete reversibility, and pose major challenges for integration with electro-optical devices. One alternative is an electrically or temperature-driven change of the surrounding medium, tuning the resonance intensity, position, and linewidth, properties which limit the achievable contrast in active metasurface applications (*21*–*29*). Yet, a nanoantenna resonance that can be turned fully ON and OFF electrically at high frequencies has not been achieved to date.

Here we introduce such electrically switchable nanoantennas, made from an optically metallic polymer with an electrochemically driven metal-to-insulator transition in the near–infrared (IR) spectral range caused by a variation of the charge carrier density. In our electrically switchable plasmonic system, the nanoantennas are made from a metallic polymer, which can be electrically switched via the applied voltage (Fig. 1A). When a voltage of +1 V is applied, the polymer is electrochemically doped and oxidized, which results in high carrier density and metallic optical properties. Consequently, the polymer nanoantenna is turned ON and exhibits a strong plasmonic nanoantenna resonance. In contrast, at an applied voltage of −1 V, the carrier density is substantially reduced and the polymer becomes insulating. The nanoantenna is switched OFF,

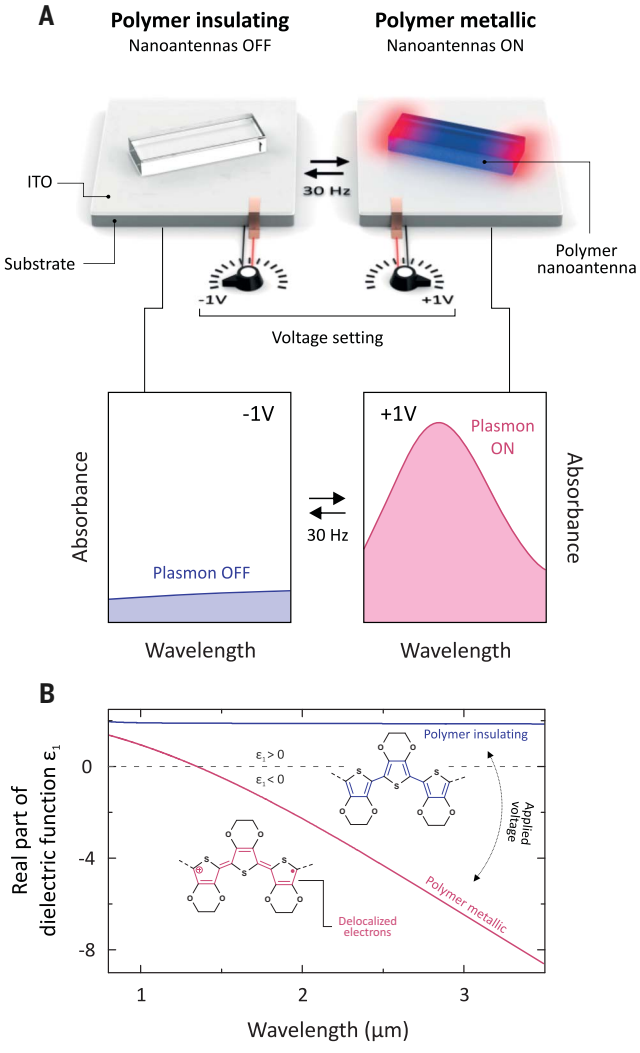

Fig. 1. Concept of electrically switchable nanoantennas made from metallic polymers with a metal-to-insulator transition. (**A**) Electrical switching of an individual metallic polymer nanoantenna. (Right) Antenna ON state at an applied voltage of +1 V. The polymer is in the metallic state and the nanoantenna exhibits a plasmonic resonance. (Left) Antenna OFF state at −1 V. The polymer becomes insulating and the nanoantenna exhibits no plasmonic resonance. Switching between the states reaches video-rate frequencies of 30 Hz. ITO (indium tin oxide) is used for electrical contacting. (**B**) Real part of the dielectric function ε_1 of the polymer in the metallic (red) and insulating (blue) states. A metallic polymer with $\varepsilon_1 < 0$ is obtained in the near-IR and mid-IR for wavelengths $\lambda > 1.3$ μm. By means of the applied voltage, the polymer can be switched into an insulating state with $\varepsilon_1 > 0$ in the entire wavelength range. (Insets) Structural conversion of the metal-to-insulator transition.

[1]4th Physics Institute and Research Center SCoPE, University of Stuttgart, Pfaffenwaldring 57, 70569 Stuttgart, Germany. [2]IPOC-Functional Polymers, Institute of Polymer Chemistry and Center for Integrated Quantum Science and Technology (IQST), University of Stuttgart, Pfaffenwaldring 55, 70569 Stuttgart, Germany.
*Corresponding author. Email: giessen@physik.uni-stuttgart.de

and no plasmonic resonance is observed. Electrical switching between the ON and OFF states occurs very rapidly, permitting video-rate switching frequencies of 30 Hz.

The core of our concept is an electrochemically driven metal-to-insulator transition of the polymer poly(3,4-ethylenedioxythiophene):polystyrene sulfonate (PEDOT:PSS). Figure 1B depicts the real part of the dielectric function ε_1 of PEDOT:PSS in its metallic (red) and insulating (blue) states, indicating this material's excellent electrical and optical properties (see fig. S1 for details). The insets of Fig. 1B illustrate the redox reaction that occurs when PEDOT:PSS changes from its neutral (insulating) state to its oxidized (bi-)polaronic (metallic) state. In detail, PEDOT:PSS is alternately oxidized and reduced, as is common in electrochemistry. Thus, applying voltages of +1 V and −1 V (versus a reference electrode) causes doping and dedoping, respectively, of the polymer and alters the charge carrier density while some hysteresis is present (see materials and methods). Higher voltages (outside of our electrochemical potential window) will cause overdoping and degradation of the material. We find that PEDOT:PSS is switchable between metallic ($\varepsilon_1 < 0$) and insulating ($\varepsilon_1 > 0$) states via the applied voltage for wavelengths >1.3 μm. The crossing $\varepsilon_1 = 0$ at $\lambda_p = 1.3$ μm defines the plasma frequency

$$\omega_p = \sqrt{ne^2/\epsilon_0 m_e}$$

below which the material is optically metallic, allowing for localized plasmonic resonances. Modifying ω_p for metallic polymers is therefore possible through manipulation of the (quasi-)free charge carrier density n (e, electron charge; ϵ_0, permittivity; m_e, electron mass). Thus, ultrahigh doping levels in metallic polymers will allow, in the future, their plasma frequency to be pushed into the visible wavelength range. Commercially available PEDOT:PSS in its pristine spin-coated state exhibits a dielectric function nearly identical to that of the oxidized metallic state. Thus, even without any applied voltage, the plasmonic properties of the metallic polymer are fully accessible. Figure S2 illustrates the fabrication and resonance tunability via geometry.

Electrical switching is carried out in a liquid environment using an electrochemical cell with a three-electrode setup (Fig. 2A; see materials and methods and fig. S5A for further information). We measured the spectral response of an array of polymer nanoantennas with length L = 300 nm for different applied voltages against the reference electrode (Fig. 2B). The pristine spectral response (dry state) and the response for +1 V are shown in gray and red, respectively. The nanoantennas exhibit a plasmonic resonance around ~2.4 μm in the dry state, as the PEDOT:PSS is almost completely oxidized and thus metallic. Applying +1 V triggers a further oxidation of PEDOT:PSS with a

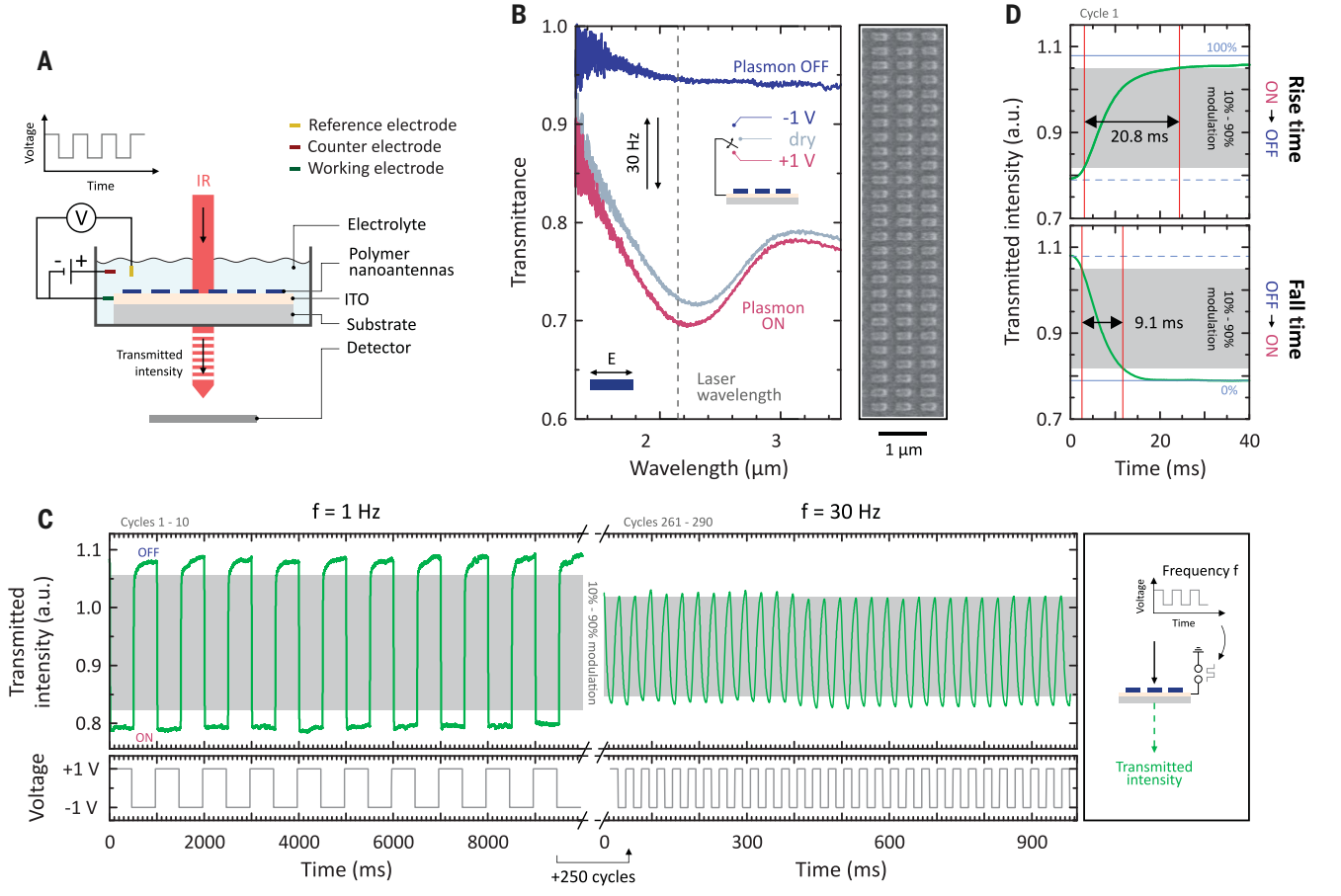

Fig. 2. Video-rate electrical switching of metallic polymer nanoantennas. (**A**) Schematic of the electrochemical cell (three-electrode setup) and optical measurement setup. (**B**) SEM image and spectral response of metallic polymer nanoantennas (length L = 300 nm, width W = 160 nm, height H = 90 nm, periodicity in x P_x = 500 nm, periodicity in y P_y = 300 nm) for different states. Dry state, pristine (gray): Plasmonic resonance almost completely turned ON. +1 V (red): Plasmonic resonance completely turned ON with highest modulation (polymer fully metallic). −1 V (blue): Plasmonic resonance turned OFF (polymer insulating). Electric field E polarized parallel to the nanoantenna long axis. The dashed line indicates the laser wavelength λ = 2.15 μm for (C) and (D). (**C**) (Top) Transmitted intensity through the polymer nanoantennas cycling between the ON and OFF states. The gray area denotes the 10% to 90% modulation window. (Bottom) Set voltage switching between +1 V and −1 V. (Left) Cycles 1 to 10 with switching frequency f = 1 Hz. (Right) Cycles 261 to 290 with f = 30 Hz. a.u., arbitrary units. (**D**) Detailed analysis of rise time τ_{rise} = 20.8 ms (ON to OFF) and fall time τ_{fall} = 9.1 ms (OFF to ON) for the first switching cycle.

maximum doping level and charge carrier density of the polymer due to the existence of (bi-)polarons (*30*, *31*). The plasmon resonance is fully turned ON with the highest possible modulation (red curve). The peak wavelength shifts slightly blue to ~2.2 μm. Notably, applying a negative voltage of −1 V (blue curve) turns the antenna resonance entirely OFF, with no remaining resonant light interaction. The PEDOT:PSS is completely reduced (i.e., in the neutral state) and hence is dielectric in the studied IR spectral range.

The switching speed of our metallic polymer nanoantennas is investigated in Fig. 2C. The antennas are switched between ON and OFF states at applied voltages of +1 V and −1 V while the transmitted intensity is recorded. The bottom graphs (gray curves) show the voltage applied to the polymer nanoantennas (±1 V), and the corresponding modulated transmitted intensity is depicted in the top graphs (green curves). The left graphs in Fig. 2C illustrate the first 10 switching cycles at a frequency of $f = 1$ Hz, confirming full transitions between the

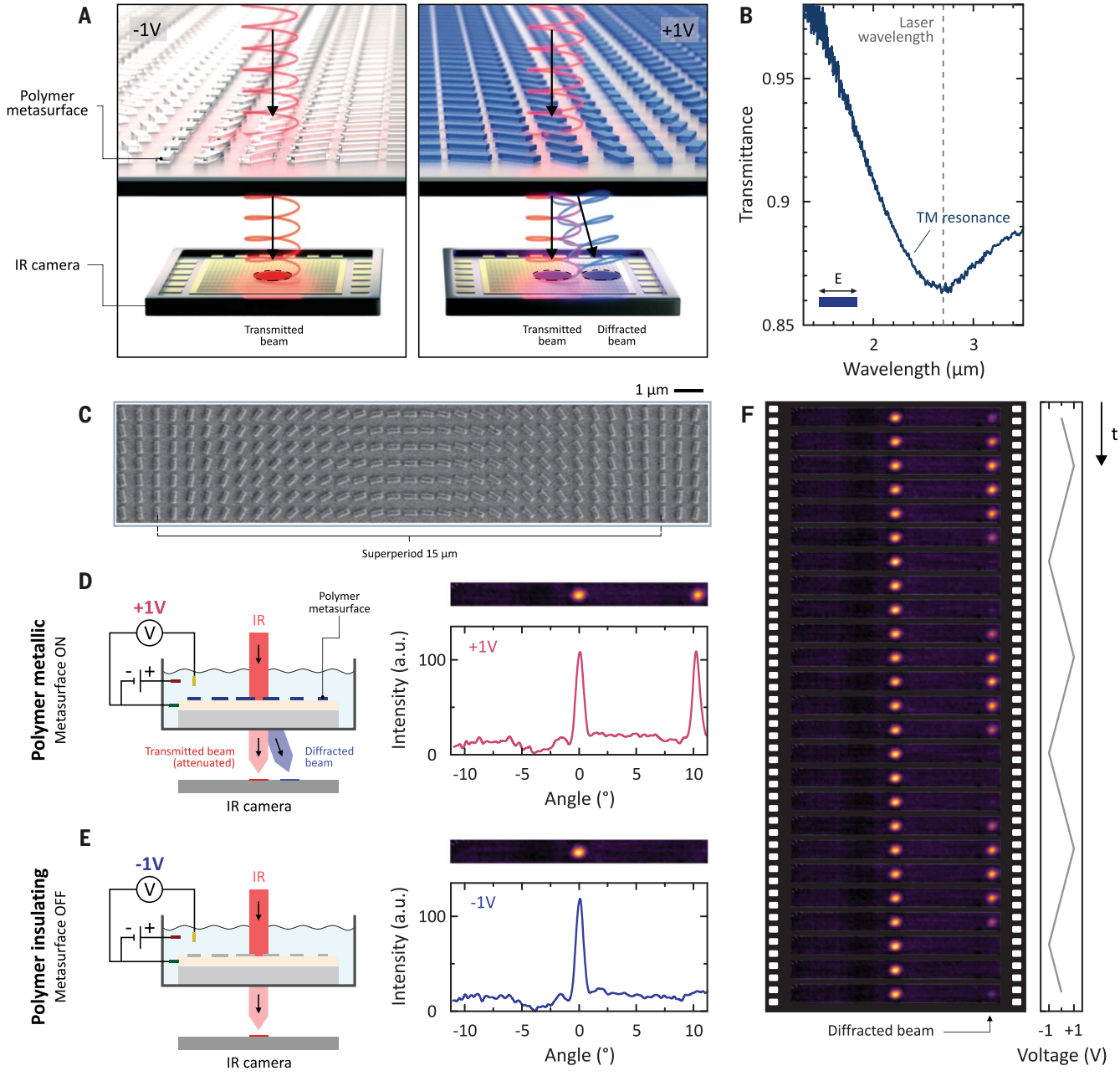

Fig. 3. Metallic polymer plasmonic metasurface for ultrahigh-contrast active beam steering. (**A**) The metallic polymer metasurface is switchable between the OFF state (−1 V, left) and the ON state (+1 V, right), thus allowing beam steering with a 100% contrast ratio in the diffracted beam. (**B** and **C**) Spectrum and SEM image of the pristine metasurface with a superperiod of 15 μm (diffraction angle $\phi = 10.2°$, L = 380 nm, W = 160 nm, H = 90 nm, $P_{x,y}$ = 500 nm). TM (transverse magnetic) plasmonic nanoantenna resonance peaking at 2.65 μm [laser wavelength in (D) to (F)]. (**D** and **E**) (Left) Schematics of the measurement setup and beam-steering concept. The metasurface is turned ON and OFF while the transmitted and diffracted beams are recorded using an IR camera. (Right) Camera images and intensity profiles in the (D) ON and (E) OFF states. The diffracted beam (right peak) at +10.2° vanishes completely for −1 V. (**F**) Selected IR camera images showing three cycles of active beam steering when the applied voltage is cycled in situ between −1 V and +1 V. The intensity of the diffracted beam (right spots) can be continuously varied depending on the applied voltage. t, time.

ON and OFF states without noticeable degradation (gray area: 10% to 90% modulation window; see fig. S5B for further information). A zoomed-in view of the first cycle is displayed in Fig. 2D. We analyze the rise time from ON to OFF (top graph) as well as the fall time from OFF to ON (bottom graph). The rise (or fall) time is defined as the time step in which the intensity rises (or falls) between 10% and 90%, respectively (red in Fig. 2D). We obtain a rise time (τ_{rise}) of 20.8 ms and a fall time (τ_{fall}) of 9.1 ms, and thus a duty cycle time (τ) of 29.9 ms, equivalent to a maximum switching frequency of f = 33 Hz. Thirty cycles of electrical switching of our plasmonic polymer nanoantennas with video-rate frequency of f = 30 Hz are depicted in the right graph of Fig. 2C (gray area: 10% to 90% modulation window, accounting for degradation of nanoantennas after 260 cycles). We find that electrical switching at video-rate frequencies is possible, as the transmitted intensity reaches beyond the 10% to 90% modulation window. The degradation after 290 switching cycles is on the order of only 25%, reducing the overall modulation (comparison of gray marked areas). Possible sources for degradation might be volume expansion of the polymer during switching and irreversible reactions during the electrochemical oxidation and reduction.

Our concept greatly boosts the integrability of plasmonic systems into, e.g., commercial smart and small-scale electro-optical devices, owing to the high switching modulation efficiency with full ON and OFF states, electrical switchability, low required voltages, and switching at video-rate frequencies. Plasmonic metasurfaces are one archetype integration of plasmonics into functional devices. As a proof of concept, we thus demonstrate an electrically switchable metallic polymer metasurface for ultrahigh-contrast active beam steering—that is, a metasurface with the ability to actively control the routing of incident light into a fixed angular range. The basic working principle is illustrated in Fig. 3A: The metasurface is illuminated with a circularly polarized light beam. Depending on the state of the polymer nanoantennas, part of the incident light is diffracted, showing opposite handedness. The key feature of our metallic polymer metasurface is the ability to fully switch it ON and OFF electrically. Consequently, the contrast ratio, defined as the ratio of the diffracted intensities in the metasurface ON and OFF states, reaches 100%.

The TM (transverse magnetic) resonance spectrum of the metallic polymer nanoantennas (the building blocks of the metasurface) peaks at 2.65 μm (Fig. 3B). A scanning electron microscopy (SEM) image of the polymer metasurface is shown in Fig. 3C. The experimental scheme is illustrated on the left in Fig. 3, D and E. The laser (right circularly polarized) is set to an illumination wavelength of 2.65 μm, and the IR camera is used to image the transmitted and diffracted intensities. See fig. S6 for further spectral and imaging information. The measured IR camera images and intensity profiles for an applied voltage of +1 V and −1 V are displayed on the right of Fig. 3, D and E (the primary transmitted beam is attenuated to prevent saturation of the IR camera). A voltage of +1 V turns the metasurface ON, and diffraction by the plasmonic polymer metasurface is observed (Fig. 3D, right). In contrast, the applied voltage of −1 V turns the metasurface completely OFF, and the diffracted beam at +10.2° vanishes completely (Fig. 3E, right). The diffraction efficiency is 1.1%. So far, the spectral contrast of the beam-steering metasurface in its ON state accounts for roughly 86% transmission versus 100% in the OFF state (Fig. 3B). This contrast is currently limiting the diffraction efficiency. Increasing the modulation depth by optimizing material, geometry, and doping levels will enhance the diffraction efficiency.

The metallic polymer nanoantennas possess another intriguing property: Successive electrochemical doping results in intermediate states between the ON and OFF states; thus, the intensity of the diffracted beam can be modified at will (Fig. 3F). We show selected IR camera images for three full switching cycles (voltage cycled between +1 V and −1 V at 20 mV/s). Whereas the primary beam remains almost unaffected, the intensity of the diffracted beam can be gradually varied between the OFF and ON states. Movie S1 shows all frames for six cycles, including the corresponding voltammograms. The diffracted beam intensities that display hysteresis behavior, which enables powerless operation in the ON or OFF state, are depicted in fig. S7.

Our electrically switchable plasmonic nanoantennas and metasurfaces enabled by metallic polymers expand the functionality and performance of plasmonic-based electro-optical active devices and on-chip optical components. Fabrication from PEDOT:PSS is low cost and scalable, owing to the commercial availability of this polymer. We envision that our concept will be of importance in several distinct fields. Subwavelength-sized polymer nanoantennas will make a sizable impact in the development of displays and active optical components. One can address individual subwavelength pixels to push the pixel densities of emerging optical technologies to entirely new dimensions. Furthermore, in comparison with state-of-the-art metallic and dielectric nanoantennas, the polymer nanoantennas allow a previously unseen level of flexibility for fabrication of curved optical devices on flexible substrates. This functionality is necessary to achieve augmented and virtual reality technologies that work in transmission (e.g., on contact lenses or glasses). Ultimately, it may even be possible to achieve pixel densities >2000 lines/mm, which would support full-color holographic movies at a very large field of view. All of these advances will be aided by nanoantenna operation at only ±1 V, which is very favorable for compatibility with low-voltage complementary metal-oxide semiconductors (CMOS) chips (0 to 3.3 V) at moderate local electric fields. From a more fundamental standpoint, current efforts in quantum technology and methodology require intricate coupling and control schemes, which can be realized via, e.g., sophisticated switchable and reconfigurable metasurfaces, which are currently out of reach even with existing state-of-the-art techniques (*32*). Such structures would allow for an entirely new level of integration and miniaturization. From a basic research point of view, further studies into the working principle of the plethora of metallic and conductive polymers will allow for fine-tuning and manipulation of their properties. This includes shifting the plasma frequency, and thus the operation point, into the visible wavelength region; increasing the switching speed for cycling beyond the demonstrated video rate; and reducing degradation. Further detailed investigations on the influence of, e.g., oxygen and humidity during electrochemical switching, adjustments to the fabrication process, and electrochemical cell sealing in inert gas environments or the use of solid electrolytes should benefit the overall switching performance. Additionally, conductive polymers have recently proven to be stable for an extremely long time, with little to no degradation over $>10^7$ cycles at video-rate switching frequencies (*33*). Metallic polymers also offer the opportunity to gradually change the carrier density and hence the plasma frequency, which allows for gray-scale operation and thus opens another window of opportunity. These results, in combination with the shown hysteresis behavior that enables powerless operation in the ON or OFF state, suggest that extremely energy-efficient display devices could be realized in the future.

REFERENCES AND NOTES

1. I. Kim *et al*., *Nat. Nanotechnol.* **16**, 508–524 (2021).
2. A. H. Dorrah, N. A. Rubin, A. Zaidi, M. Tamagnone, F. Capasso, *Nat. Photonics* **15**, 287–296 (2021).
3. G. Y. Lee *et al*., *Nat. Commun.* **9**, 4562 (2018).
4. J. Park *et al*., *Nat. Nanotechnol.* **16**, 69–76 (2021).
5. W.-J. Joo *et al*., *Science* **370**, 459–463 (2020).
6. N. Yu *et al*., *Science* **334**, 333–337 (2011).
7. L. Huang *et al*., *Nano Lett.* **12**, 5750–5755 (2012).
8. A. V. Kildishev, A. Boltasseva, V. M. Shalaev, *Science* **339**, 1232009 (2013).
9. M. Khorasaninejad *et al*., *Science* **352**, 1190–1194 (2016).
10. S. Wang *et al*., *Nat. Nanotechnol.* **13**, 227–232 (2018).
11. A. Arbabi, Y. Horie, M. Bagheri, A. Faraon, *Nat. Nanotechnol.* **10**, 937–943 (2015).
12. X. Ni, N. K. Emani, A. V. Kildishev, A. Boltasseva, V. M. Shalaev, *Science* **335**, 427 (2012).
13. A. M. Shaltout, V. M. Shalaev, M. L. Brongersma, *Science* **364**, eaat3100 (2019).
14. M. Wuttig, H. Bhaskaran, T. Taubner, *Nat. Photonics* **11**, 465–476 (2017).
15. S. Chen *et al*., *Nat. Nanotechnol.* **15**, 35–40 (2020).
16. Q. Wang *et al*., *Nat. Photonics* **10**, 60–65 (2016).
17. J. Karst *et al*., *Sci. Adv.* **6**, eaaz0566 (2020).
18. F. Sterl *et al*., *Nano Lett.* **15**, 7949–7955 (2015).
19. Y. Wang *et al*., *Nat. Nanotechnol.* **16**, 667–672 (2021).
20. Y. Zhang *et al*., *Nat. Nanotechnol.* **16**, 661–666 (2021).

21. G. K. Shirmanesh, R. Sokhoyan, P. C. Wu, H. A. Atwater, *ACS Nano* **14**, 6912–6920 (2020).
22. J. Li, P. Yu, S. Zhang, N. Liu, *Nat. Commun.* **11**, 3574 (2020).
23. T. Xu *et al*., *Nat. Commun.* **7**, 10479 (2016).
24. J. Peng *et al*., *Sci. Adv.* **5**, eaaw2205 (2019).
25. S. Q. Li *et al*., *Science* **364**, 1087–1090 (2019).
26. J. Ratzsch *et al*., *J. Opt.* **22**, 124001 (2020).
27. Y. Leroux *et al*., *ACS Nano* **2**, 728–732 (2008).
28. R. Kaissner *et al*., *Sci. Adv.* **7**, eabd9450 (2021).
29. X. Yin *et al*., *Light Sci. Appl.* **6**, e17016 (2017).
30. D. Neusser *et al*., *Chem. Mater.* **32**, 6003–6013 (2020).
31. M. Wieland *et al*., *Flex. Print. Electron.* **5**, 014016 (2020).
32. A. S. Solntsev, G. S. Agarwal, Y. S. Kivshar, *Nat. Photonics* **15**, 327–336 (2021).
33. K. Xiong *et al*., *Adv. Mater.* **2103217**, e2103217 (2021).

ACKNOWLEDGMENTS

We thank F. Sterl and F. Mörz for contributions to the experimental setup and L.-S. Hornberger and B. Gompf for contributions to the ellipsometry measurements. **Funding:** We acknowledge financial support from Baden-Wuerttemberg-Stiftung (Opterial), the European Research Council (ERC Advanced Grant Complexplas and ERC PoC Grant 3DPrintedOptics), Bundesministerium für Bildung und Forschung, Deutsche Forschungsgemeinschaft (SPP1839 Tailored Disorder and GRK2642 Photonic Quantum Engineers), the Institute of Quantum Science and Technology (IQST), the University of Stuttgart (Terra Incognita), the Carl Zeiss Foundation, and the Vector Foundation. **Author contributions:** J.K., M.H., and H.G. conceived the project. J.K. and M.U. fabricated the samples. J.K. and M.F. performed the measurements. J.K. carried out the data analysis. C.D., C.M., and T.S. contributed to the experimental setup, sample fabrication, and measurements. H.G., M.H., and S.L. supervised the project. All authors discussed the results and contributed to manuscript writing. **Competing interests:** J.K., M.H., and H.G. have filed an international patent related to the topic of this work (PCT/EP2021/069202). **Data and materials availability:** All data needed to evaluate the conclusions in the paper are present in the paper and/or the supplementary materials.

SUPPLEMENTARY MATERIALS

science.org/doi/10.1126/science.abj3433
Materials and Methods
Figs. S1 to S7
Reference (*34*)
Movie S1

10 July 2021; accepted 13 September 2021
10.1126/science.abj3433